ACS NANO

www.acsnano.org

ARTICLE

Route to Enhancing Remote Epitaxy of Perovskite Complex Oxide Thin Films

Sangho Lee,[¶] Xinyuan Zhang,[¶] Pooya Abdollahi, Matthew R. Barone, Chengye Dong, Young Jin Yoo, Min-Kyu Song, Doyoon Lee, Jung-El Ryu, Jun-Hui Choi, Jae-Hyun Lee, Joshua A. Robinson, Darrell G. Schlom, Hyun S. Kum, Celesta S. Chang,* Ambrose Seo,* and Jeehwan Kim*

Cite This: *ACS Nano* 2024, 18, 31225–31233

Read Online

ACCESS | Metrics & More | Article Recommendations | Supporting Information

ABSTRACT: **Remote epitaxy is taking center stage in creating freestanding complex oxide thin films with high crystallinity that could serve as an ideal building block for stacking artificial heterostructures with distinctive functionalities. However, there exist technical challenges, particularly in the remote epitaxy of perovskite oxides associated with their harsh growth environments, making the graphene interlayer difficult to survive. Transferred graphene, typically used for creating a remote epitaxy template, poses limitations in ensuring the yield of perovskite films, especially when pulsed laser deposition (PLD) growth is carried out, since graphene degradation can be easily observed. Here, we employ spectroscopic ellipsometry to determine the critical factors that damage the integrity of graphene during PLD by tracking the change in optical properties of graphene *in situ*. To mitigate the issues observed in the PLD process, we propose an alternative growth strategy based on molecular beam epitaxy to produce single-crystalline perovskite membranes.**

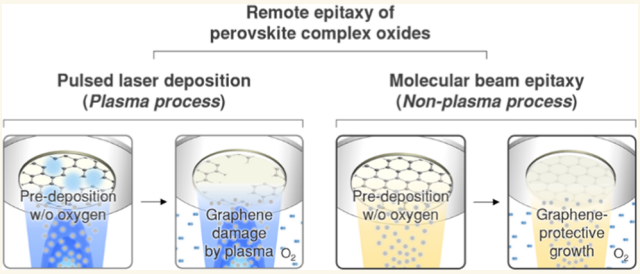

KEYWORDS: *remote epitaxy, complex oxide, graphene, thin film, pulsed laser deposition, molecular beam epitaxy, spectroscopic ellipsometry*

Remote epitaxy is a burgeoning growth technique of single-crystalline thin films on atomically thin two-dimensional (2D) materials like graphene.[1−10] This has set the stage for producing epitaxial films that can be easily released from slippery 2D surfaces and transferred onto arbitrary substrates of interest.[1−3,5,6,8,9] Among a wide range of materials demonstrated for remote epitaxy, complex oxides, including spinel, garnet, and perovskite, have garnered particular interest due to their inherently high ionic character and unusual functionalities.[3,11] The underlying principle behind remote epitaxy suggests that the polarity or ionicity of materials strongly governs a distant atomic interaction between the substrate and epilayer through the graphene interlayer, making complex oxides suitable for remote epitaxy even with using bilayer graphene.[3,12] Also, freestanding complex oxide membranes peeled off from 2D surfaces can show exceptional electronic, magnetic, and optical properties compared to the counterpart films bound to substrates owing to the absence of substrate clamping.[3,13,14] Furthermore, by integrating dissimilar functional oxide layers with no lattice and processing restrictions, we expect to create exotic interfaces with emergent phenomena attributed to the unusual physical coupling in these artificial heterostructures.[3,15−18]

Despite such compelling opportunities in the remote epitaxy of complex oxides, it faces some technical challenges, specifically for oxides that typically necessitate extremely harsh processing conditions unsuited for preserving the graphene interlayer during their growth. For example, pulsed laser deposition (PLD), an archetypal and widely used epitaxy technique for complex oxide growth, involves a high-energy plasma plume generated when the laser beam hits the PLD target (source material) for depositing thin films, making graphene highly susceptible for degradation.[3,19,20] This becomes more severe if it requires a highly elevated growth temperature (T_{growth}) and oxygen pressure (P_{O2}) to grow single-crystalline thin films, which critically limits the remote epitaxy of oxides. For instance, optimal T_{growth} and P_{O2} for perovskites, such as $SrTiO_3$ (STO) and $BaTiO_3$ (BTO), are relatively high, ranging from 850 to 900 °C and 50 to 100

Received: July 14, 2024
Revised: October 10, 2024
Accepted: October 17, 2024
Published: October 29, 2024

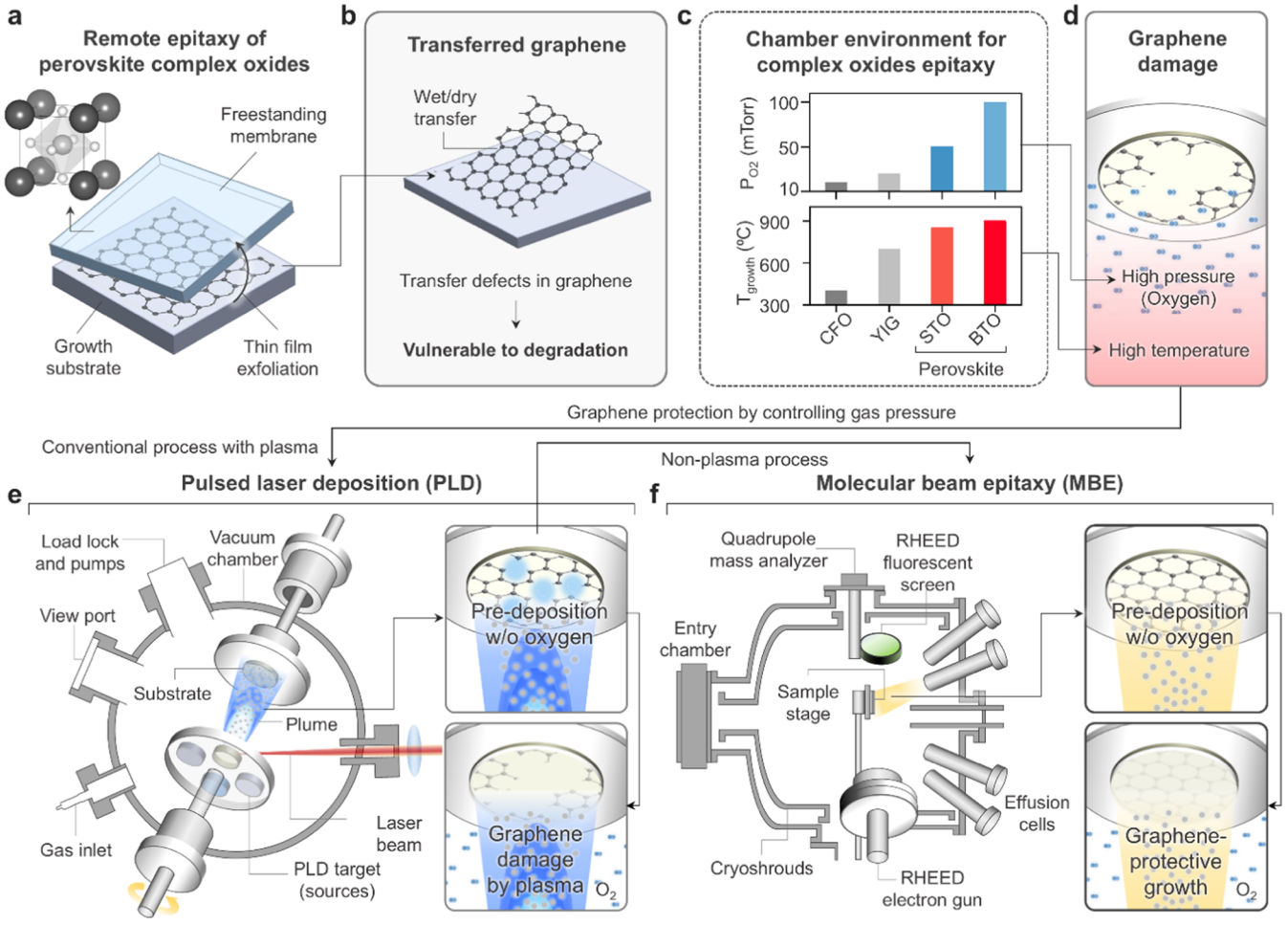

Figure 1. Remote epitaxy of perovskite complex oxides through transferred graphene. (a) Perovskite remote epitaxy based on (b) transferred graphene-coated growth template. (c) Optimal T_{growth} and P_{O2} conditions for complex oxides epitaxy and (d) graphene damage during perovskite growth due to harsh chamber environment. (e) PLD- and (f) MBE-based graphene-protective growth process for remote epitaxy.

mTorr, respectively.[3] Such conditions accelerate graphene damage while growing these films. As a strategy to protect graphene, an ultrathin buffer can be grown under a vacuum ($<5 \times 10^{-6}$ Torr) during the first minutes of deposition to avoid direct exposure to a harsh O_2 plasma environment.[3,21] However, a plasma plume at such a high T_{growth} can still break sp^2-bonded carbon atoms in graphene even at a sufficiently low chamber pressure.[20]

Another major limitation is the technical difficulty in creating a growth template for complex oxides with an atomically clean 2D surface. Graphene has been the most widely used 2D interlayer for remote epitaxy due to its transparency, allowing distant atomic interaction between the substrate and epilayer. Synthesizing uniform, thickness-controlled mono- to bilayer graphene directly on complex oxide surfaces is known to be intrinsically challenging.[22,23] Therefore, its transfer process from appropriate substrates is typically used to form graphene on target substrates.[24,25] However, this procedure inevitably introduces a significant number of unwanted defects, such as wrinkles, holes, process residues, and interfacial contamination.[26] These can disturb the remote interaction of the substrate with the epilayer, thereby reducing the crystal quality and exfoliation yield of complex oxide thin films.[19]

In this work, we identify the key technical obstacles in the remote epitaxy of complex oxide (especially perovskite) thin films on graphene-coated growth substrates, mainly associated with the graphene transfer process and PLD-based oxide growth condition. An *in situ* optical characterization technique, called spectroscopic ellipsometry, is employed to monitor how graphene behaves in a PLD growth environment while deposited STO vapor species are nucleated on its surface at different T_{growth}. Based on our in-depth study, we set the possible growth regime for graphene to survive when using PLD and propose molecular beam epitaxy (MBE) as an alternative approach for accomplishing the remote epitaxy of oxides that require high-temperature growth, such as BTO thin films. Moreover, we investigate how graphene crystallinity and transfer methods affect the BTO film quality.

RESULTS AND DISCUSSION

We elaborate on the process flow in Figure 1 for perovskite thin film remote epitaxy, where transferred graphene is used as the interlayer. As illustrated in Figure 1a,b, the growth template, a graphene-coated crystalline oxide substrate, is typically formed via wet or dry transfer of graphene onto a target substrate[24,25] (see the Methods section for detailed processes). Both methods are likely to introduce transfer defects in graphene, which makes it vulnerable to further physical degradation during oxide growth, resulting in a low remote epitaxial film quality. Meanwhile, every class of

https://doi.org/10.1021/acsnano.4c09445
ACS Nano 2024, 18, 31225−31233

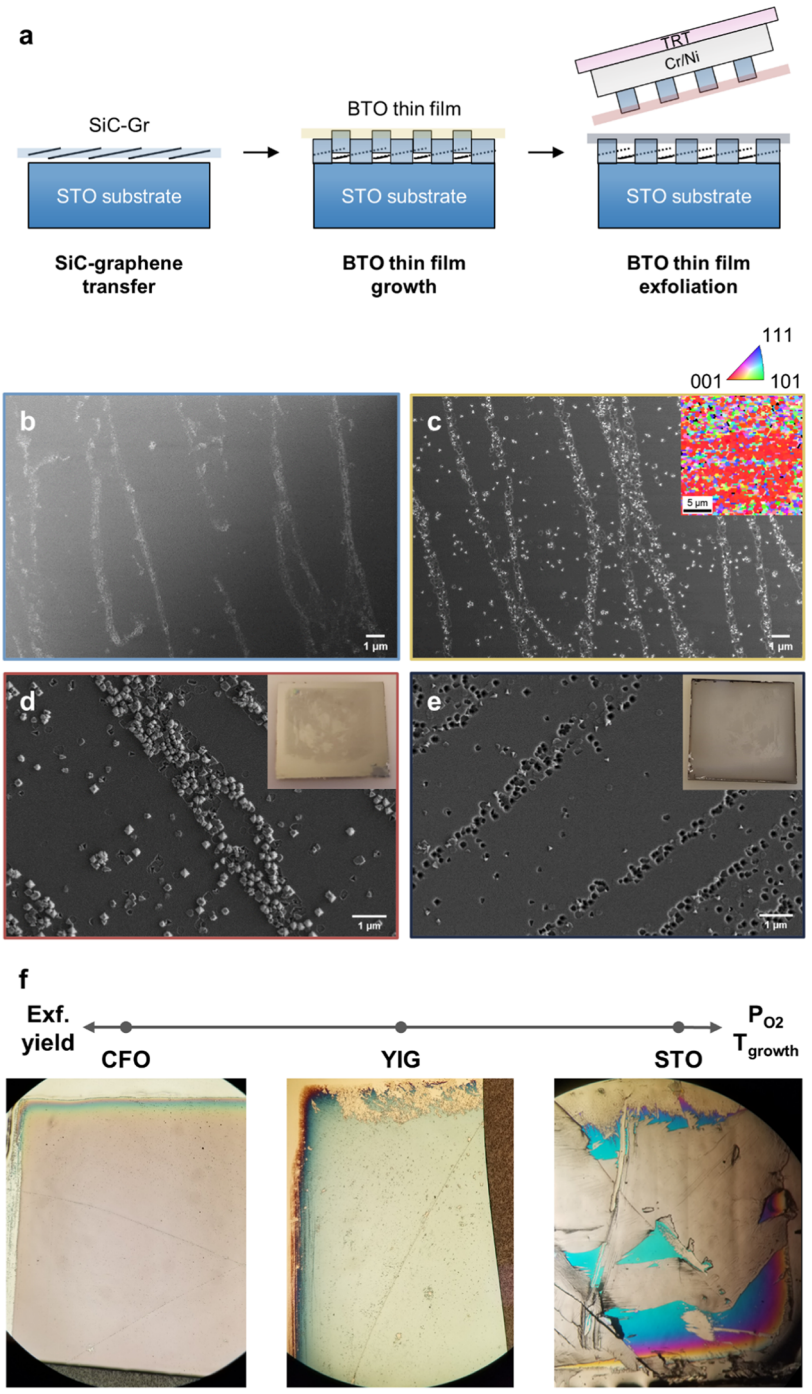

Figure 2. Challenges in remote epitaxy of perovskite complex oxides using PLD. (a) Schematic of freestanding BTO membrane generation by remote epitaxy. Top-view SEM images are shown following the process of remote epitaxy and exfoliation: (b) dry-transferred SiC-graphene on STO substrate, (c) BTO thin film grown on graphene-coated STO substrate, (d) exfoliated film side, and (e) remaining substrate side after BTO lift-off, exhibiting different morphology depending on graphene regional quality. Inset: (c) EBSD orientation map of BTO film grown on graphene. Low magnification photographs of (d) exfoliated film side and (e) remaining substrate after BTO exfoliation. (f) Photographs of remote epitaxial CFO (left), YIG (middle), and STO (right) membranes released from substrates. The exfoliation yield of the membrane shows a decreasing trend as P_{O2} and T_{growth} required for single-crystal growth increase.

complex oxide materials has its own optimal chamber environment to produce a single-crystalline thin film, mostly represented by T_{growth} and P_{O2}, as described in Figure 1c. We note that perovskite (*e.g.*, STO and BTO) requires significantly higher values in both T_{growth} and P_{O2} than those of spinel (*e.g.*, $CoFe_2O_4$ or CFO) and garnet (*e.g.*, $Y_3Fe_5O_{12}$ or YIG). As T_{growth} and P_{O2} increase, graphene is more drastically damaged during thin film growth due to a higher incident energy given to its surface. This poses a critical challenge in achieving a high yield of perovskite thin films (Figure 1d). To mitigate this issue, around 5 to 10 nm thick buffer layers can be incorporated without oxygen overpressure to cover the graphene surface before growing the actual film in an optimized P_{O2}. When such a strategy is performed under

https://doi.org/10.1021/acsnano.4c09445
ACS Nano 2024, 18, 31225−31233

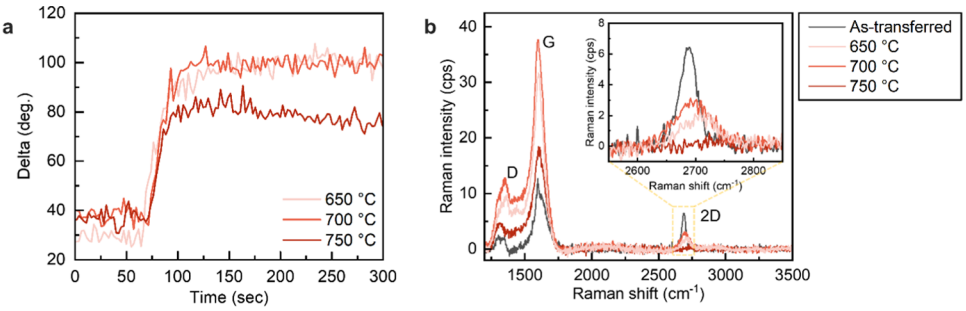

Figure 3. Effect of T_{growth} on graphene degradation during PLD growth of STO buffer under vacuum. (a) Spectroscopic ellipsometry dynamical spectra taken of the delta at 1.5 eV while STO vapor species are nucleated on the graphene surface and (b) Raman spectra of graphene acquired after STO buffer growth at different T_{growth}. PLD growth of the STO buffer layer starts at the 60-s mark, where the Delta value jumps abruptly.

vacuum (<5 × 10^{-6} Torr), it was demonstrated that the following film growth in the optimum condition does not etch graphene while maintaining single crystallinity even on the buffer.[3] However, particularly in the case of perovskite remote epitaxy that requires high T_{growth}, the application of this approach is severely limited, as graphene degradation could still be observed even with no oxygen flow. As depicted in Figure 1e, predeposition of the buffer layer with no P_{O2} does not fully preserve the graphene interlayer owing to the seemingly high-energy plasma at the augmented temperature introduced in perovskite oxide growth via PLD. Thus, it requires a narrow processing window and precise control of graphene thickness and quality to obtain a single-crystalline perovskite membrane with a high exfoliation yield. On the other hand, MBE, an epitaxy technique based on the thermal evaporation of material species, typically shows an incident energy orders of magnitude lower than that of PLD, offering a graphene-protective growth strategy that works better for remote epitaxy of perovskite thin films (Figure 1f).

Figure 2 presents the aforementioned challenges in the remote epitaxy of 100 nm thick perovskite oxides when using the PLD technique. As illustrated in the schematic process in Figure 2a, dry-transferred epitaxial graphene (*e.g.*, SiC-graphene) was used as a remote epitaxy template for BTO thin film growth, since this induces fewer transfer defects and higher crystallinity compared to wet-transferred polycrystalline graphene.[7,19] However, SiC-graphene exhibits bilayer stripes by its nature,[27] which leads to a thickness variation across graphene-coated STO substrate (Figure 2b). Such atomic-thickness difference in graphene can still affect how much electrostatic potential of the substrate is penetrated through graphene, which determines the quality of the BTO thin film. Also, regions with monolayer graphene are more susceptible to deterioration under harsh BTO growth conditions in PLD. Even when the graphene-protective growth strategy discussed earlier is introduced, it can instantly etch one atom thick graphene during the growth of the protective buffer layer. Therefore, remote epitaxy of BTO thin film on transferred SiC-graphene produced polycrystalline BTO particulates that were formed along the bilayer stripe region, while most other areas showed single-crystalline BTO film directly grown on bare STO substrate, resulting from etched graphene (Figure 2c). When an attempt was made to exfoliate this BTO film via the deposition of a Cr/Ni stressor layer, only those particles were released from the substrate due to weak bonding with the remaining graphene underneath, and the rest of the film was strongly bound to the substrate side (Figures 2d,e and S1).

As presented in Figure 1c, both T_{growth} and P_{O2} required for complex oxide growth show an increasing trend from spinel CFO, garnet YIG, to perovskite STO, which is closely tied to the exfoliation yield of their remote epitaxial films. The more severe the oxide growth environment is, the more difficult it is for graphene to survive during remote epitaxy, reducing the area of released membranes with atomically smooth surfaces. Thus, the exfoliation yield of the CFO and YIG membranes was higher than 90%, while only a small portion of the STO membrane was successfully lifted off, as described in Figure 2f. Even when using thicker graphene (more than bilayer) to enhance its membrane yield for STO remote epitaxy, the crystal quality of a well-exfoliated STO membrane was poor, and it still exhibited a considerable area of spalled region (Figure S2). Since the plume generated in the PLD environment does not etch graphene precisely at the level of atomic scale thickness, it is not guaranteed to form a uniform van der Waals (vdW) gap at the graphene interface across the substrate after STO growth, which limits its controllability over remote epitaxy. Moreover, it is likely to build up more transfer defects when preparing thick graphene layers via multiple transfer processes, further interrupting distant atomic interactions between the substrate and epilayer.

To identify which parameter of PLD growth is the major cause of graphene degradation, the temperature effect was first checked by using *in situ* spectroscopic ellipsometry. In Figure S3, we performed real-time monitoring of SiC-graphene on STO substrate, a remote epitaxy template for perovskite oxides, placed inside the PLD chamber while elevating its temperature from room temperature up to 950 °C under vacuum (<1 × 10^{-6} Torr). We note that graphene did not show any noticeable change in the spectra during thermal cycling, indicating that graphene can be intact even at the high T_{growth} (850−900 °C) required for perovskite epitaxy under vacuum. On the other hand, under moderate oxygen partial pressure (P_{O2} = 10 mTorr), the optical spectra started to show a drop at low photon energies when heating the sample, demonstrating that graphene is easily damaged at lower temperatures between 100 and 200 °C in the presence of oxygen gas.

For this reason, ultrathin buffer grown under a vacuum should be introduced, especially for the high-temperature remote epitaxy process. However, the above experiments lack the details of the precise damage onset temperature and the actual processing window under a real growth environment when using the PLD technique. For *in situ* observation in this study, we utilized PLD equipped with a spectral ellipsometry

https://doi.org/10.1021/acsnano.4c09445
ACS Nano 2024, 18, 31225−31233

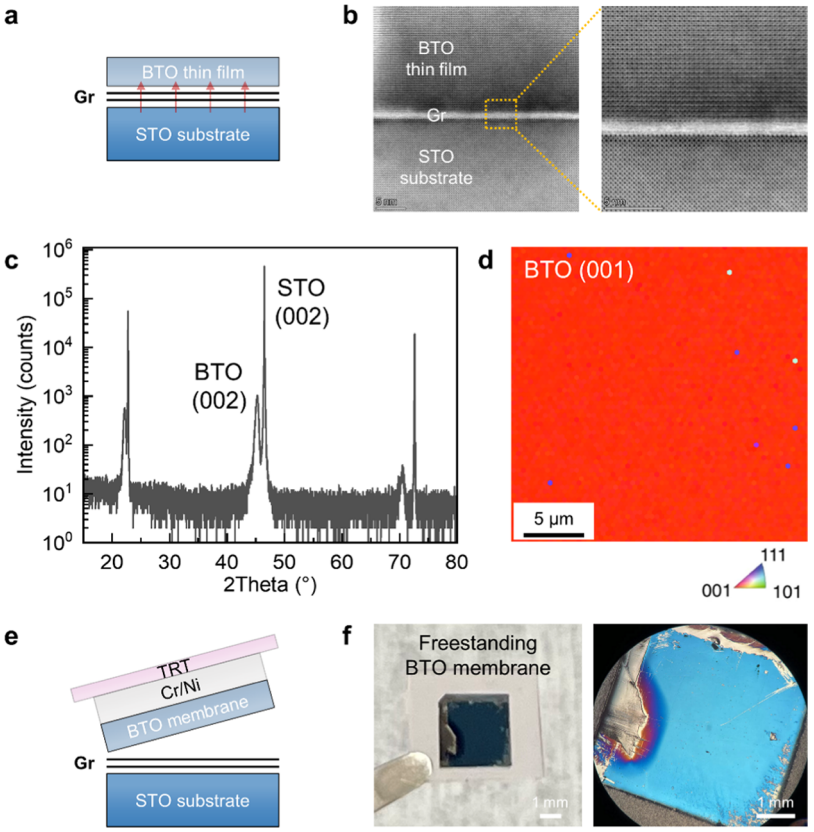

Figure 4. Remote epitaxy of BTO thin film via MBE. (a) Schematic, (b) cross-sectional annular bright-field (ABF)-STEM image, (c) 2θ-ω XRD scan, and (d) EBSD orientation map of BTO film grown on bilayer graphene-coated STO substrate. Using the exfoliation method described in panel (e), the BTO membrane was exfoliated from a bilayer graphene-coated STO platform, as displayed in panel (f).

setup and acquired real-time optical data. We first observed the nucleation of the STO buffer layer on graphene under vacuum ($<1 \times 10^{-6}$ Torr) at different T_{growth}. As described in Figure 3a, delta (Δ) values at 1.5 eV exhibited a slightly increasing tendency at T_{growth} of 650 and 700 °C when 2−3 nm thick STO buffer was grown on graphene for 120 s, whereas after STO growth for ∼90 s at 750 °C, it decreased instead. This indicates that graphene damage becomes more apparent at T_{growth} = 750 °C, which confirms the difficulty of forming a buffer at such a high T_{growth} with the graphene intact. *Ex situ* Raman spectroscopy analysis of the graphene layer after STO buffer growth shows good agreement with these *in situ* ellipsometry measurement results (Figure 3b). We note that the 2D peak in the Raman spectrum disappeared at T_{growth} = 750 °C, where the graphene was completely etched away. Due to accelerated graphene degradation under the combination of harsh plasma and high-temperature environment, it is challenging to pursue a graphene-protective strategy using PLD when T_{growth} over 750 °C is required.

As delineated in Figure 1f, the MBE technique is suggested as an alternative route to offer milder processing to minimize graphene damage, enabling successful perovskite remote epitaxy. Owing to its relatively low-energy process without direct exposure to a plasma plume, MBE is compatible with the graphene-protective strategy even in high-temperature epitaxy conditions. In Figure 4, we demonstrated the MBE-based remote epitaxy of BTO thin film on bilayer SiC-graphene-coated STO substrate, which requires the harshest growth environment within complex oxides to generate a single-crystalline film. Here, we first found the optimal T_{growth} required for producing a single-crystalline BTO thin film as well as for lifting it off from the substrate (Figure S4). At this T_{growth}, a uniform vdW gap created by the graphene interlayer was preserved after BTO film growth, as shown in Figures 4a,b and S5. We also confirmed remote epitaxial interaction taking place even across bilayer graphene, leading to a distant atomic alignment between the BTO film and the underlying STO substrate. Single crystallinity of this remote epitaxial BTO film over a large area was proved by 2θ-ω X-ray diffraction (XRD) scan and electron backscatter diffraction (EBSD) mapping in Figure 4c,d. Furthermore, we showed that a few millimeter-sized freestanding BTO membranes can be released from graphene-coated STO substrate with higher than 90% exfoliation yield, which verifies greater suitability of MBE-based remote epitaxy for perovskite oxides (Figure 4e,f).

Using the same epitaxy process via MBE, we investigated the effect of graphene crystallinity and its transfer method on the remote epitaxial perovskite film quality. As discussed earlier, polycrystalline or single-crystalline graphene can be formed on the target substrate using wet or dry transfer to generate a growth template, consisting of a graphene-covered oxide substrate. In the case of single-crystalline graphene epitaxially grown on SiC substrate, the dry transfer method based on mechanical exfoliation is more favorable than chemically etching the entire rigid substrate.[25] Polycrystalline graphene chemically synthesized on Cu foil and Ge substrate are typically wet- and dry-transferred onto oxide substrate, respectively.[24,28] Depending on the graphene quality and its transfer process, there was a clear difference in crystallinity of BTO epilayer grown on graphene, represented by the full

https://doi.org/10.1021/acsnano.4c09445
ACS Nano 2024, 18, 31225−31233

width at half-maximum (fwhm) of X-ray rocking curves for BTO (002) thin films with a thickness of 50 nm (Figure 5a).

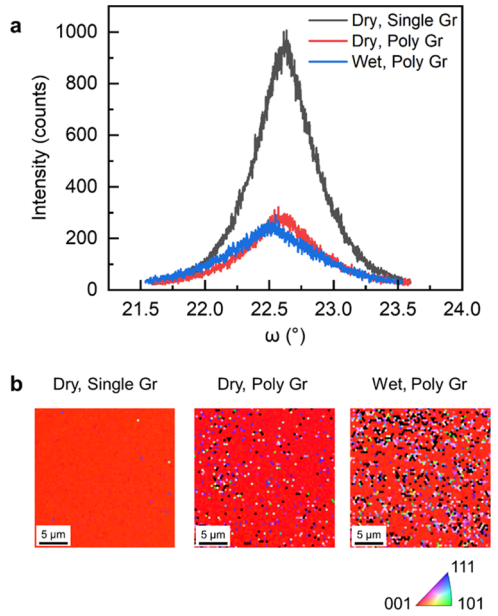

Figure 5. Dependence of BTO membrane quality on graphene crystallinity and transfer method. (a) Rocking curves and (b) EBSD orientation maps of BTO thin films grown on different graphene-based remote epitaxy templates; Dry, Single Gr, dry-transferred single-crystalline graphene; Dry, Poly Gr, dry-transferred polycrystalline graphene; Wet, Poly Gr, wet-transferred polycrystalline graphene.

First, the fwhm value was lower for BTO film on single-crystalline graphene (0.57°) than on polycrystalline graphene (0.64°), showing its better quality. This is because single-crystalline graphene is more robust and uniform over a larger area compared to polycrystalline graphene, thereby promoting long-range order growth of remote epitaxial BTO film. In addition, BTO grown on dry-transferred graphene exhibited a significantly lower fwhm value than that of wet-transferred graphene case (0.84°). As the dry transfer method is less likely to introduce wrinkles and residues in graphene than the wet transfer process, it facilitates more effective remote interaction between epilayer and substrate across graphene, leading to high-quality BTO film. This trend was also observed in EBSD mapping results in Figure 5b, showing a nearly perfect film crystallinity for the BTO layer on dry-transferred, single-crystalline graphene, presumably due to a negligible number of transfer defects. It was further confirmed in 2θ-ω XRD scans in Figure S6 that only this graphene template provided a single-crystal BTO film, while others displayed the additional XRD peaks of BTO (111) and (110) orientations.

CONCLUSIONS

Our study shows that the current growth templates relying on transferred graphene for remote epitaxy of complex oxide thin films cannot provide atomically clean interfaces, essential for guaranteeing high crystal quality and exfoliation yield. To avoid such issues attributed to transfer defects, we emphasize the importance of developing direct synthesis methods for high-quality graphene on growth substrates. We believe this could play a pivotal role specifically in enabling remote epitaxy of perovskite oxides even when using the PLD process owing to greatly improved control over the thickness, uniformity, and scalability of graphene. Further developments of defect-free, wafer-scale vdW surfaces herein could serve as an ideal remote epitaxy platform for the high-throughput production of single-crystalline complex oxide (including perovskite) membranes in a scalable and controlled manner. Furthermore, this will lay the foundation for the facile fabrication of a diverse class of mixed-dimensional heterogeneous systems that exhibit emergent physical phenomena at their well-defined interfaces.

METHODS

Preparation of Remote Epitaxy Templates. For graphene-based remote epitaxy templates, single-crystalline graphene on the SiC substrate and polycrystalline graphene on the Ge substrate and Cu foil were transferred onto crystalline oxide substrates, including STO, $MgAl_2O_4$ (MAO), and $Gd_3Ga_5O_{12}$ (GGG). More details concerning the synthesis or growth of graphene can be found in refs 7,19. SiC-graphene and Ge-graphene were mechanically exfoliated by a Ni stressor layer and transferred onto a target substrate using the standard dry transfer method.[25] Cu-graphene was wet-transferred by chemically etching Cu foil in $FeCl_3$ solution and scooping graphene layer by oxide substrate.[24]

Remote Epitaxy of Complex Oxide Thin Films. PLD was employed to remote epitaxially grow complex oxide thin films (CFO, YIG, STO, and BTO) on graphene-coated oxide substrates using a KrF excimer laser (λ = 248 nm) with 1.3 J/cm^2 fluence. The initial 500 shots with a pulse rate of 2 Hz were deposited prior to active layer growth under vacuum (<5 × 10^{-6} Torr) at a set temperature of 400, 700, 850, and 900 °C to grow buffer layers of CFO, YIG, STO, and BTO, respectively. The actual temperature of the substrate was measured to be about 150−200 °C lower than the set temperature. The actual film was subsequently grown on the buffer with a pulse rate of 10 Hz at the same set temperature as the buffer growth condition but under different oxygen partial pressures (P_{O2} = 10, 20, 50, and 100 mTorr for CFO, YIG, STO, and BTO, respectively). All films here were cooled under the same P_{O2} conditions, in which actual films were grown until the substrate temperature was below 200 °C.

MBE was used for the remote epitaxy of BTO thin films on graphene-covered STO substrates by using a Veeco GEN10 MBE system. Source materials of elemental Ba and Ti in conventional effusion cells were used to generate molecular beams of Ba and Ti to synthesize BTO, and their fluxes were calibrated by monitoring the reflection high-energy electron diffraction (RHEED) pattern to deposit stoichiometric BTO. Graphene-coated substrates were heated in ultrahigh vacuum up to set temperatures in the range of 900 to 1050 °C. As a graphene-protective growth strategy, the O_2 oxidant was supplied with a background pressure of 1 × 10^{-6} Torr after the growth temperature was reached, and the shutters to the Ba and Ti sources were simultaneously opened for a predetermined time to grow a targeted thickness of BTO. The time taken to complete 1 unit cell of BTO growth was found to be 29 s based on the RHEED oscillation calibration. All films here were cooled in the same P_{O2} in which they were grown until the substrate temperature was below 200 °C. More details concerning BTO remote epitaxy via MBE can be found in ref 29.

Remote Epitaxial Complex Oxide Membrane Exfoliation. The remote epitaxial CFO, YIG, STO, and BTO thin films were mechanically peeled off of the graphene-coated oxide substrates. After a Cr adhesion layer was deposited, followed by a Ni stressor layer on oxide epilayers, a thermal release tape (TRT) was subsequently attached on top as a support layer. The resultant TRT/Ni/Cr/epilayer stacks were peeled off at the graphene interface to generate freestanding oxide membranes.

MATERIALS CHARACTERIZATION

The morphology and crystallinity of the top or exfoliated surface of remote epitaxial oxide thin films were analyzed by a ZEISS Merlin high-resolution scanning electron microscope (SEM) equipped with

https://doi.org/10.1021/acsnano.4c09445
ACS Nano 2024, 18, 31225−31233

an EBSD detector, using an electron beam voltage of 15 kV, and the samples were tilted at 70° with a working distance of 15 mm. The structural properties of oxide thin films were characterized by high-resolution XRD, using a Rigaku SmartLab high-resolution diffractometer with Cu Kα_1 radiation (λ = 1.5406 Å) as an X-ray source and an incident beam Ge-(220) double-bounce monochromator. Raman spectra of graphene on STO substrates were obtained after STO buffer growth on top, using a Raman microscopic system (α 300M+, WITec) with a pump laser wavelength of 532 nm. Details on cross-sectional scanning transmission electron microscopy (STEM) characterization can be found in ref 29.

***In Situ* Optical Spectroscopic Ellipsometry.** The real-time optical properties of our samples were measured during the PLD of STO buffer layers on SiC-graphene/STO substrates at different temperatures. The PLD system is equipped with *in situ* optical spectroscopic ellipsometry (Woollam M-2000−210), consisting of the light source (a Xe lamp) and analyzer assemblies mounted to the vacuum chamber (base pressure of around 10^{-7} Torr) with an incident angle of 65° relative to the sample's normal axis.[30] Experimental ellipsometric angle spectra, $\Psi(\omega)$ and $\Delta(\omega)$, were taken every 2 s by averaging 80 dynamic scans (*i.e.*, 40 Hz) in the spectral range of 1.2−5.9 eV in photon energy. Ψ and Δ stand for the differential changes in amplitude and phase experienced upon reflection by the two *p*- and *s*-polarization components, expressed by the ratio of Fresnel reflection coefficients ($\tilde{R}_p$ and $\tilde{R}_s$): $\rho \equiv \frac{\tilde{R}_p}{\tilde{R}_s} = \tan\Psi e^{i\Delta}$. Since spectroscopic ellipsometry is a self-normalizing technique, there is no need for separate measurements of optical reference samples. The Δ values with 1.5 eV incident photons, shown in Figure 3, were plotted as a function of time at different temperatures during PLD of the STO buffer layer.

ASSOCIATED CONTENT

Supporting Information

The Supporting Information is available free of charge at https://pubs.acs.org/doi/10.1021/acsnano.4c09445.

Additional information on SEM images showing morphologies of exfoliated film and remaining substrate, EBSD maps and photographs for exfoliated film, *in situ* optical spectroscopic ellipsometry of graphene/substrate, cross-sectional STEM images for film/graphene/substrate, and 2θ-ω XRD scans for remote epitaxial film (PDF)

AUTHOR INFORMATION

Corresponding Authors

Jeehwan Kim − *Department of Mechanical Engineering, Massachusetts Institute of Technology, Cambridge, Massachusetts 02139, United States; Research Laboratory of Electronics and Department of Materials Science and Engineering, Massachusetts Institute of Technology, Cambridge, Massachusetts 02139, United States;* orcid.org/0000-0002-1547-0967; Email: jeehwan@mit.edu

Ambrose Seo − *Department of Physics and Astronomy, University of Kentucky, Lexington, Kentucky 40506, United States;* orcid.org/0000-0002-7055-5314; Email: a.seo@uky.edu

Celesta S. Chang − *Department of Physics and Astronomy, Seoul National University, Seoul 08826, Republic of Korea*; Email: celesta@snu.ac.kr

Authors

Sangho Lee − *Department of Mechanical Engineering, Massachusetts Institute of Technology, Cambridge, Massachusetts 02139, United States; Research Laboratory of Electronics, Massachusetts Institute of Technology, Cambridge, Massachusetts 02139, United States;* orcid.org/0000-0003-4164-1827

Xinyuan Zhang − *Research Laboratory of Electronics and Department of Materials Science and Engineering, Massachusetts Institute of Technology, Cambridge, Massachusetts 02139, United States*

Pooya Abdollahi − *Department of Physics and Astronomy, University of Kentucky, Lexington, Kentucky 40506, United States*

Matthew R. Barone − *Department of Materials Science and Engineering, Cornell University, Ithaca, New York 14850, United States;* orcid.org/0000-0003-1221-181X

Chengye Dong − *Department of Materials Science and Engineering and 2-Dimensional Crystal Consortium, The Pennsylvania State University, University Park, Pennsylvania 16802, United States*

Young Jin Yoo − *Department of Mechanical Engineering, Massachusetts Institute of Technology, Cambridge, Massachusetts 02139, United States; Research Laboratory of Electronics, Massachusetts Institute of Technology, Cambridge, Massachusetts 02139, United States;* orcid.org/0000-0002-6490-2324

Min-Kyu Song − *Department of Mechanical Engineering, Massachusetts Institute of Technology, Cambridge, Massachusetts 02139, United States; Research Laboratory of Electronics, Massachusetts Institute of Technology, Cambridge, Massachusetts 02139, United States;* orcid.org/0000-0002-9233-9356

Doyoon Lee − *Research Laboratory of Electronics and Department of Materials Science and Engineering, Massachusetts Institute of Technology, Cambridge, Massachusetts 02139, United States*

Jung-El Ryu − *Department of Mechanical Engineering, Massachusetts Institute of Technology, Cambridge, Massachusetts 02139, United States; Research Laboratory of Electronics, Massachusetts Institute of Technology, Cambridge, Massachusetts 02139, United States*

Jun-Hui Choi − *Department of Energy Systems Research and Department of Materials Science and Engineering, Ajou University, Suwon 16499, Republic of Korea*

Jae-Hyun Lee − *Department of Energy Systems Research and Department of Materials Science and Engineering, Ajou University, Suwon 16499, Republic of Korea;* orcid.org/0000-0001-5117-8923

Joshua A. Robinson − *Department of Materials Science and Engineering and 2-Dimensional Crystal Consortium, The Pennsylvania State University, University Park, Pennsylvania 16802, United States*

Darrell G. Schlom − *Department of Materials Science and Engineering, Cornell University, Ithaca, New York 14850, United States;* orcid.org/0000-0003-2493-6113

Hyun S. Kum − *Department of Electrical and Electronic Engineering, Yonsei University, Seoul 03722, Republic of Korea*

Complete contact information is available at: https://pubs.acs.org/10.1021/acsnano.4c09445

Author Contributions

[¶]S.L. and X.Z. equally contributed to this work.

https://doi.org/10.1021/acsnano.4c09445
ACS Nano 2024, 18, 31225−31233

Notes

The authors declare no competing financial interest.

ACKNOWLEDGMENTS

This work is supported by the Global-LAMP Program of the National Research Foundation of Korea (NRF) grant funded by the Ministry of Education (no. RS-2023-00301976) and the NRF grant funded by the Korea Government (MSIT) (no. RS-2024-00355333). P.A. and A.S. acknowledge the support of the National Science Foundation (NSF) (grant no. DMR-2104296) for *in situ* optical spectroscopy. C.D. and J.A.R. acknowledge support from the 2-Dimensional Crystal Consortium—Materials Innovation Platform (2DCC-MIP) (grant no. NSF DMR-1539916).

REFERENCES

(1) Kim, Y.; Cruz, S. S.; Lee, K.; Alawode, B. O.; Choi, C.; Song, Y.; Johnson, J. M.; Heidelberger, C.; Kong, W.; Choi, S.; Qiao, K.; Almansouri, I.; Fitzgerald, E. A.; Kong, J.; Kolpak, A. M.; Hwang, J.; Kim, J. Remote epitaxy through graphene enables two-dimensional material-based layer transfer. *Nature* **2017**, *544*, 340−343.

(2) Jiang, J.; Sun, X.; Chen, X.; Wang, B.; Chen, Z.; Hu, Y.; Guo, Y.; Zhang, L.; Ma, Y.; Gao, L.; Zheng, F.; Jin, L.; Chen, M.; Ma, Z.; Zhou, Y.; Padture, N. P.; Beach, K.; Terrones, H.; Shi, Y.; Gall, D.; et al. Carrier lifetime enhancement in halide perovskite via remote epitaxy. *Nat. Commun.* **2019**, *10*, No. 4145.

(3) Kum, H. S.; Lee, H.; Kim, S.; Lindemann, S.; Kong, W.; Qiao, K.; Chen, P.; Irwin, J.; Lee, J. H.; Xie, S.; Subramanian, S.; Shim, J.; Bae, S.-H.; Choi, C.; Ranno, L.; Seo, S.; Lee, S.; Bauer, J.; Li, H.; Lee, K.; et al. Heterogeneous integration of single-crystalline complex-oxide membranes. *Nature* **2020**, *578*, 75−81.

(4) Bae, S.-H.; Lu, K.; Han, Y.; Kim, S.; Qiao, K.; Choi, C.; Nie, Y.; Kim, H.; Kum, H. S.; Chen, P.; Kong, W.; Kang, B.-S.; Kim, C.; Lee, J.; Baek, Y.; Shim, J.; Park, J.; Joo, M.; Muller, D. A.; Lee, K.; Kim, J. Graphene-assisted spontaneous relaxation towards dislocation-free heteroepitaxy. *Nat. Nanotechnol.* **2020**, *15*, 272−276.

(5) Jeong, J.; Wang, Q.; Cha, J.; Jin, D. K.; Shin, D. H.; Kwon, S.; Kang, B. K.; Jang, J. H.; Yang, W. S.; Choi, Y. S.; Yoo, J.; Kim, J. K.; Lee, C.-H.; Lee, S. W.; Zakhidov, A.; Hong, S.; Kim, M. J.; Hong, Y. J. Remote heteroepitaxy of GaN microrod heterostructures for deformable light-emitting diodes and wafer recycle. *Sci. Adv.* **2020**, *6*, No. eaaz5180.

(6) Qiao, K.; Liu, Y.; Kim, C.; Molnar, R. J.; Osadchy, T.; Li, W.; Sun, X.; Li, H.; Myers-Ward, R. L.; Lee, D.; Subramanian, S.; Kim, H.; Lu, K.; Robison, J. A.; Kong, W.; Kim, J. Graphene buffer layer on SiC as a release layer for high-quality freestanding semiconductor membranes. *Nano Lett.* **2021**, *21*, 4013−4020.

(7) Kim, H.; Chang, C. S.; Lee, S.; Jiang, J.; Jeong, J.; Park, M.; Meng, Y.; Ji, J.; Kwon, Y.; Sun, X.; Kong, W.; Kum, H. S.; Bae, S.-H.; Lee, K.; Hong, Y. J.; Shi, J.; Kim, J. Remote epitaxy. *Nat. Rev. Methods Primers.* **2022**, *2*, No. 40.

(8) Yoon, H.; Truttmann, T. K.; Liu, F.; Matthews, B. E.; Choo, S.; Su, Q.; Saraswat, V.; Manzo, S.; Arnold, M. S.; Bowden, M. E.; Kawasaki, J. K.; Koester, S. J.; Spurgeon, S. R.; Chambers, S. A.; Jalan, B. Freestanding epitaxial $SrTiO_3$ nanomembranes via remote epitaxy using hybrid molecular beam epitaxy. *Sci. Adv.* **2022**, *8*, No. eadd5328.

(9) Kim, H.; Liu, Y.; Lu, K.; Chang, C. S.; Sung, D.; Akl, M.; Qiao, K.; Kim, K. S.; Park, B.-I.; Zhu, M.; Suh, J. M.; Kim, J.; Jeong, J.; Baek, Y.; Ji, Y. J.; Kang, S.; Lee, S.; Han, N. M.; Kim, C.; Choi, C.; et al. High-throughput manufacturing of epitaxial membranes from a single wafer by 2D materials-based layer transfer process. *Nat. Nanotechnol.* **2023**, *18*, 464−470.

(10) Park, B.-I.; Kim, J.; Lu, K.; Zhang, X.; Lee, S.; Suh, J. M.; Kim, D.-H.; Kim, H.; Kim, J. Remote Epitaxy: Fundamentals, Challenges, and Opportunities. *Nano Lett.* **2024**, *24*, 2939−2952.

(11) Ji, J.; Park, S.; Do, H.; Kum, H. S. A review on recent advances in fabricating freestanding single-crystalline complex-oxide membranes and its applications. *Phys. Scr.* **2023**, *98*, No. 052002.

(12) Kong, W.; Li, H.; Qiao, K.; Kim, Y.; Lee, K.; Nie, Y.; Lee, D.; Osadchy, T.; Molnar, R. J.; Gaskill, D. K.; Myers-Ward, R. L.; Daniels, K. M.; Zhang, Y.; Sundram, S.; Yu, Y.; Bae, S.-H.; Rajan, S.; Shao-Horn, Y.; Cho, K.; Ougazzaden, A.; et al. Polarity governs atomic interaction through two-dimensional materials. *Nat. Mater.* **2018**, *17*, 999−1004.

(13) Brewer, A.; Lindemann, S.; Wang, B.; Maeng, W.; Frederick, J.; Li, F.; Choi, Y.; Thompson, P. J.; Kim, J. W.; Mooney, T.; Vaithyanathan, V.; Schlom, D. G.; Rzchowski, M. S.; Chen, L. Q.; Ryan, P. J.; Eom, C. B. Microscopic piezoelectric behavior of clamped and membrane (001) PMN-30PT thin films. *Appl. Phys. Lett.* **2021**, *119*, No. 202903.

(14) Shi, Q.; Parsonnet, E.; Cheng, X.; Fedorova, N.; Peng, R.-C.; Fernandez, A.; Qualls, A.; Huang, X.; Chang, X.; Zhang, H.; Pesquera, D.; Das, S.; Nikonov, D.; Young, I.; Chen, L.-Q.; Martin, L. W.; Huang, Y.-L.; Íñiguez, J.; Ramesh, R. The role of lattice dynamics in ferroelectric switching. *Nat. Commun.* **2022**, *13*, No. 1110.

(15) Wang, J. J.; Yang, T. N.; Wang, B.; Rzchowski, M. S.; Eom, C. B.; Chen, L. Q. Strain-Induced Interlayer Parallel-to-Antiparallel Magnetic Transitions of Twisted Bilayers. *Adv. Theory Simul.* **2021**, *4*, No. 2000215.

(16) Li, Y.; Xiang, C.; Chiabrera, F. M.; Yun, S.; Zhang, H.; Kelly, D. J.; Dahm, R. T.; Kirchert, C. K. R.; Cozannet, T. E. L.; Trier, F.; Christensen, D. V.; Booth, T. J.; Simonsen, S. B.; Kadkhodazadeh, S.; Jespersen, T. S.; Pryds, N. Stacking and twisting of freestanding complex oxide thin films. *Adv. Mater.* **2022**, *34*, No. 2203187.

(17) Sánchez-Santolino, G.; Rouco, V.; Puebla, S.; Aramberri, H.; Zamora, V.; Cabero, M.; Cuellar, F. A.; Munuera, C.; Mompean, F.; Garcia-Hernandez, M.; Castellanos-Gomez, A.; Íñiguez, J.; Leon, C.; Santamaria, J. A 2D ferroelectric vortex pattern in twisted BaTiO3 freestanding layers. *Nature* **2024**, *626*, 529−534.

(18) Han, S.; Kim, J. S.; Park, E.; Meng, Y.; Xu, Z.; Foucher, A. C.; Jung, G. Y.; Roh, I.; Lee, S.; Kim, S. O.; Moon, J.-Y.; Kim, S.-I.; Bae, S.; Zhang, X.; Park, B.-I.; Seo, S.; Li, Y.; Shin, H.; Reidy, K.; Hoang, A. T.; et al. High energy density in artificial heterostructures through relaxation time modulation. *Science* **2024**, *384*, 312−317.

(19) Kim, H.; Lu, K.; Liu, Y.; Kum, H. S.; Kim, K. S.; Qiao, K.; Bae, S.-H.; Lee, S.; Ji, Y. J.; Kim, K. H.; Paik, H.; Xie, S.; Shin, H.; Choi, C.; Lee, J. H.; Dong, C.; Robinson, J. A.; Lee, J.-H.; Ahn, J.-H.; Yeom, G. Y.; et al. Impact of 2D−3D heterointerface on remote epitaxial interaction through graphene. *ACS Nano* **2021**, *15*, 10587−10596.

(20) Wohlgemuth, M. A.; Trstenjak, U.; Sarantopoulos, A.; Gunkel, F.; Dittmann, R. Control of growth kinetics during remote epitaxy of complex oxides on graphene by pulsed laser deposition. *APL Mater.* **2024**, *12*, No. 021113.

(21) Yan, X.; Cao, H.; Li, Y.; Hong, H.; Gosztola, D. J.; Guisinger, N. P.; Zhou, H.; Fong, D. D. In situ x-ray studies of growth of complex oxides on graphene by molecular beam epitaxy. *APL Mater.* **2022**, *10*, No. 091114.

(22) Sun, J.; Gao, T.; Song, X.; Zhao, Y.; Lin, Y.; Wang, H.; Ma, D.; Chen, Y.; Xiang, W.; Wang, J.; Zhang, Y.; Liu, Z. Direct growth of high-quality graphene on high-κ dielectric $SrTiO_3$ substrates. *J. Am. Chem. Soc.* **2014**, *136*, 6574−6577.

(23) Kim, K. S.; Kang, J. E.; Chen, P.; Kim, S.; Ji, J.; Yeom, G. Y.; Kim, J.; Kum, H. S. Atomic layer-by-layer etching of graphene directly grown on $SrTiO_3$ substrates for high-yield remote epitaxy and lift-off. *APL Mater.* **2022**, *10*, No. 041105.

(24) Suk, J. W.; Kitt, A.; Magnuson, C. W.; Hao, Y.; Ahmed, S.; An, J.; Swan, A. K.; Goldberg, B. B.; Ruoff, R. S. Transfer of CVD-grown monolayer graphene onto arbitrary substrates. *ACS Nano* **2011**, *5*, 6916−6924.

(25) Kim, J.; Park, H.; Hannon, J. B.; Bedell, S. W.; Fogel, K.; Sadana, D. K.; Dimitrakopoulos, C. Layer-resolved graphene transfer via engineered strain layers. *Science* **2013**, *342*, 833−836.

(26) Kong, W.; Kum, H.; Bae, S.-H.; Shim, J.; Kim, H.; Kong, L.; Meng, Y.; Wang, K.; Kim, C.; Kim, J. Path towards graphene

commercialization from lab to market. *Nat. Nanotechnol.* **2019**, *14*, 927−938.
(27) Emtsev, K. V.; Bostwick, A.; Horn, K.; Jobst, J.; Kellogg, G. L.; Ley, L.; McChesney, J. L.; Ohta, T.; Reshanov, S. A.; Röhrl, J.; Rotenberg, E.; Schmid, A. K.; Waldmann, D.; Weber, H. B.; Seyller, T. Towards wafer-size graphene layers by atmospheric pressure graphitization of silicon carbide. *Nat. Mater.* **2009**, *8*, 203−207.
(28) Lee, J.-H.; Lee, E. K.; Joo, W.-J.; Jang, Y.; Kim, B.-S.; Lim, J. Y.; Choi, S.-H.; Ahn, S. J.; Ahn, J. R.; Park, M.-H.; Yang, C.-W.; Choi, B. L.; Hwang, S.-W.; Whang, D. Wafer-scale growth of single-crystal monolayer graphene on reusable hydrogen-terminated germanium. *Science* **2014**, *344*, 286−289.
(29) Chang, C. S.; Kim, K. S.; Park, B.-I.; Choi, J.; Kim, H.; Jeong, J.; Barone, M.; Parker, N.; Lee, S.; Zhang, X.; Lu, K.; Suh, J. M.; Kim, J.; Lee, D.; Han, N. M.; Moon, M.; Lee, Y. S.; Kim, D.-H.; Schlom, D. G.; Hong, Y. J.; Kim, J. Remote epitaxial interaction through graphene. *Sci. Adv.* **2023**, *9*, No. eadj5379.
(30) Gruenewald, J. H.; Nichols, J.; Seo, S. S. A. Pulsed laser deposition with simultaneous *in situ* real-time monitoring of optical spectroscopic ellipsometry and reflection high-energy electron diffraction. *Rev. Sci. Instrum.* **2013**, *84*, No. 043902.

https://doi.org/10.1021/acsnano.4c09445
ACS Nano 2024, 18, 31225−31233